

FLUID-SOLID INTERACTIVE MODELLING OF FABRIC-BASED ATMOSPHERIC ENTRY SIZED AERODYNAMIC DECELARATORS

Emanuel Malof and Javid Bayandor

CRashworthiness for Aerospace Structures and Hybrids (CRASH) Lab
 Department of Mechanical and Aerospace Engineering
 University at Buffalo – The State University of New York, New York 14260, USA

Abstract

Despite humble origins, fabric-based parachutes are still the main way to decelerate aircraft, landing vehicles and rockets. However, experimental testing of parachutes is expensive and impractical for various canopy shapes and opening velocities. Numerical methods offer an alternative to these costly experiments and provide analyses in a wide range of environments. Fluid-Structural Interaction is utilised to model the deployment, inflation, and descent of a parachute. This paper utilises explicit time-marching finite-element and computational fluid dynamics codes to model the deployment process of a parachute from flat to fully inflated. A hemispherical Air Force type parachute and the annular NASA Curiosity rover parachute were modelled to benchmark the state-of-the-art in inflation computational modelling to existing experimental data. Overall, this paper offers three main areas of focus. First, a study into the effects of penalty-based versus Lagrangian contact algorithms to limit fabric impingement with a hybridised model. Second, a comparison of geometric-based cloth modelling techniques to physical-based strategies to improve parachute folding and unfurling. And third, parachute inflation simulation for two models at multiple entry velocities utilising both Large Eddy Simulation and a pressure-based numerical method. By improving parachute inflation simulation methods, the accuracy of modelling the deployment of parachutes of various designs is greatly increased.

Keywords: Parachute, Aerodynamic Decelerator, Atmospheric Entry, Fluid Structural Interaction (FSI), Large Eddy Simulations (LES)

1. Introduction

Dating back to 1783 [1], parachute designs and materials have continuously improved. Due to their numerous applications throughout the aerospace field, formal parachute experimental testing has been conducted since the 1950s, beginning at the Wright Air Development Center in Ohio [2]. The results from the thousands of these tests would become the standard for aerodynamic decelerator data. However, due to the lack of computational power and the highly nonlinear physics associated with parachutes, experimental testing was expensive in terms of time, energy and safety. Additionally, due to the vast amount of parachute parameters and materials, the ability to repeatedly test multiple parachute designs was limited [2]. Numerical analysis of parachutes offers an alternative to experimental testing. Simulating parachutes of different designs in a wide range of environments allows for the prediction of complex parachute dynamics, thereby saving time and cost throughout the parachute development process. Although documentation exists on the interactions of an already unfurled parachute with its environment, research into modelling of a fully packed to fully deployed parachute remains limited. This study aims at initially utilising various numerical methods to simulate the inflation process of two different parachute geometries at multiple entry velocities, from flat to fully deployed.

2. Theory

2.1 Drag and Reynolds Number

Parachute inflation physics is highly nonlinear due to the turbulent flow that develops within and around the parachute canopy. Additionally, there exists unsteady flow separation and large deformations and stresses within the thin structure of the parachute fabric [3]. Despite these complexities, the actual modelling of the flow relies mostly on the Reynolds Number, *Re* [4].

Re is the ratio of the inertial forces to viscous forces in a fluid experiencing movement due to different internal velocities. In the highly turbulent flow region of the "internal area" of the parachute, the high Re experienced (physical data ranging from 85,539 to 357,250) is not as applicable [5]. Therefore, the unit Re^* , which better represents the effects of the viscosity on the fluid, is more relevant [6]. Equation (1) represents the unit Re equation, where p = fluid density, u = fluid velocity, and p = fluid dynamic viscosity. This equation is almost identical to the regular Re equation, but divided by the characteristic length, L, to get a nondimensionalised value. In the simulation, the characteristic length is simply the diameter of the cylindrical fluid domain (parachute canopy).

$$Re^* = \frac{\rho u}{\mu} \tag{1}$$

Whilst the unit Re governs the fluid characteristics, the drag force on the parachute fabric is the primary method of reducing the velocity of the payload. Equation (2) defines the drag, where D = drag force, q = dynamic pressure, S = surface area, $C_D = coefficient of drag$, $D_{Desc} = drag during descent$, and W = payload/parachute weight.

$$D = qSC_D; \left(q = \frac{\rho u^2}{2}\right); D_{Desc} = W$$
 (2)

At a stable vertical descent after inflation, the drag force is just equal to the weight of the parachute and the payload [3]. Numerical methods determine the drag force on each element of the parachute canopy during the inflation process, while the drag force in wind tunnel experiments is calculated by finding the normal forces incident on the fabric via pressure sensors. By comparing the total drag force from wind tunnel test data with simulation results, the aerodynamic decelerator models can be verified. Further verification can be achieved by utilising parachute equations developed by Knacke [5]. Developed in the 1950s, these empirical equations can be used to compare set values in the parachute inflation simulation to ensure that the simulation is following a reasonable trend.

$$F_A = q_S C_D S C_X X_1 \; ; \; t_f = \frac{8D_o}{V_S^{0.9}} \tag{3}$$

In Eq. (3), the parachute opening force, F_A , and the fill time, t_f , represent two factors unique to each parachute geometry and entry velocity that can be used as further verification with simulation values. Other variables include q_s = dynamic pressure at line stretch, D_o = nominal diameter and V_s = velocity at lines stretch. Here, line stretch denotes the time during the inflation process at which the parachute cables fully extend and begin to stretch in tension. The opening load factor, C_X , and the force reduction factor, X_1 , are constants determined from the empirical data of Knacke's numerous parachute experiments. Although these values only exist for their respective experimental prototypes, when simulating these designs, it can provide further verification when compared to the manually calculated values for each model [7]. Future work on the simulations present in this report will focus on extending these equations to new parachute designs.

2.2 Numerical Methods

Simulations of parachute inflation models reduce the need for expensive parachute experiments, but the mathematics involved in these analyses are extraordinarily complex. Thus, numerical methods must be utilised to approximate the associated parachute physics. Instead of moving the parachute through the fluid, the parachute cables are anchored to a fixed point near the velocity inlet while the slack parachute is inflated via the moving fluid. To accurately model the inflation, first both the parachute fabric and domain around the unfurling parachute must be meshed. This discretisation process is further explained in the methodology section. The intricacies of the turbulent flow during the simulation require the implementation of two different numerical methods, one to resolve the turbulence and one to solve the Navier-Stokes equations for each fluid element.

Although the Reynolds-Averaged Navier-Stokes (RANS) equations and Shear Stress Transport (SST) turbulence models are useful for modelling turbulent incompressible flows, they are inaccurate when compared to Direct Numerical Simulation (DNS) [8]. In DNS, the Navier-Stokes equations for the flow field are directly solved for without the use of a turbulence model.

The inaccurate RANS models of the turbulent eddies within the parachute canopy led to fabric impingement and incorrect inflation of the parachute. However, DNS remains computationally expensive and impractical for repeat aerodynamic decelerator simulations. Large Eddy Simulation (LES) was instead used as an alternate mathematical model for the turbulence, due to its robustness when simulating turbulent flows compared to RANS, but decreased computational time when compared to DNS [9]. Initially developed in 1963 to simulate atmospheric air currents, LES is better tailored for modelling the intricacies of the turbulent air trapped within the parachute canopy [9]. The LES model utilises low-pass filtering of the applied Navier-Stokes equations to remove infinitesimally small air currents within the fluid mesh that can cause singularities within the fluid domain as well as the parachute fabric. LES focuses on directly simulating large eddies influenced by the geometry in the flow, whilst modelling the smaller eddies using a subgrid-scale (SGS) model. The LES filter is presented in Eq. (4), where $\phi(\mathbf{x}, t)$ represents any flow variable from the discretised spatial and temporal field (in this case velocity and pressure). G simply represents the filter convolution matrix or the array of the adjusted values of the fluid elements after filtering.

$$\overline{\phi(\mathbf{x},t)} = \int_{-\infty}^{\infty} \int_{-\infty}^{\infty} \phi(\mathbf{r},\tau) G(\mathbf{x}-\mathbf{r},t-\tau) d\tau d\mathbf{r}$$
 (4)

In the simulation, the slow speeds of the initial parachute reentry (<100 m/s) allow for the air to be treated as incompressible. Equation (5) represents the filtered incompressible continuity equation whilst Eq. (6) is the filtered Navier-Stokes equation for momentum, where a bar above a variable denotes filtering. This is achieved by applying the LES filter to the incompressible fluid field: $\rho u(x, t)$.

$$\frac{\partial \overline{u_i}}{\partial x_i} = 0 \tag{5}$$

$$\frac{\partial \overline{u_i}}{\partial x_i} = 0$$

$$\frac{\partial u_i}{\partial t} + \frac{\partial u_i u_j}{\partial x_j} = -\frac{1}{\rho} \frac{\partial P}{\partial x_i} + \nu \frac{\partial^2 u_i}{\partial x_j \partial x_j} \rightarrow \frac{\partial \overline{u_i}}{\partial t} + \frac{\overline{\partial u_i u_j}}{\partial x_j} = -\frac{1}{\rho} \frac{\partial \overline{P}}{\partial x_i} + \nu \frac{\partial^2 \overline{u_i}}{\partial x_j \partial x_j}$$
(6)

The computational solver calculates the filtered variables, but the unfiltered variables in the equation are unknown. However, through substitution, the incalculable variables can be replaced with the known filtered variables. This substitution is demonstrated in Eq. (7).

$$\frac{\overline{\partial u_{l}u_{j}}}{\partial x_{j}} = ??; \frac{\partial \overline{u}_{l}\overline{u}_{j}}{\partial x_{j}} = Known; : Substitute$$

$$\frac{\partial \overline{u}_{l}}{\partial t} + \frac{\partial \overline{u}_{l}\overline{u}_{j}}{\partial x_{j}} = -\frac{1}{\rho} \frac{\partial \overline{P}}{\partial x_{i}} + \nu \frac{\partial^{2} \overline{u}_{l}}{\partial x_{j}\partial x_{j}} - \left(\frac{\overline{\partial u_{l}u_{j}}}{\partial x_{j}} - \frac{\partial \overline{u}_{l}\overline{u}_{j}}{\partial x_{j}}\right) \tag{7}$$

A final substitution with the expression for the shear stress, shown in Eq. 8, gives the final LES equation for incompressible flow, Eq. 9. This LES approach simplifies the turbulent eddies within the fluid domain to better model the parachute inflation with a reduced penalty to computational time.

$$\tau_{ij} = \overline{u_i u_j} - \overline{u_i} \overline{u_j} \tag{8}$$

$$\tau_{ij} = \overline{u_i u_j} - \overline{u_i} \overline{u_j}$$

$$\frac{\partial \overline{u_i}}{\partial t} + \overline{u_j} \frac{\partial \overline{u_i}}{\partial x_j} = -\frac{1}{\rho} \frac{\partial \overline{P}}{\partial x_i} + \nu \frac{\partial^2 \overline{u_i}}{\partial x_j \partial x_j} - \frac{\partial \tau_{ij}}{\partial x_j}$$

$$\tag{9}$$

With the large-scale eddies resolved and small-scale eddies modeled using SGS modelling, the Navier-Stokes equations can be solved for each element. Thus, a second-order pressure-based numerical method is utilised as it has historically been used to better model incompressible flows [10]. More specifically, the Pressure-Implicit with Splitting Operators (PISO) algorithm is used as opposed to the Semi-Implicit Method for Pressure Linked Equations (SIMPLE) model, since the PISO solver is more robust when solving transient cases with large timesteps [11].

The PISO algorithm solves the filtered momentum equation for each fluid element by utilising a pressure-velocity calculation procedure that involves one predictor step and two corrector steps. The boundary conditions of the fluid field are used to solve the momentum equations (velocity and mass flux) for each fluid element. These in turn are used to solve the pressure-correction equations, which are applied to update the mass flux, pressure, and velocity values to satisfy the continuity equation. Next, the filtered turbulence energies are incorporated, and the equations are repeatedly solved until the solution converges and the solver moves on to the next time step. The flowchart demonstrated in Figure 1 helps to visualise this process that repeats the individual steps of the algorithm until convergence, at which point the algorithm is terminated.

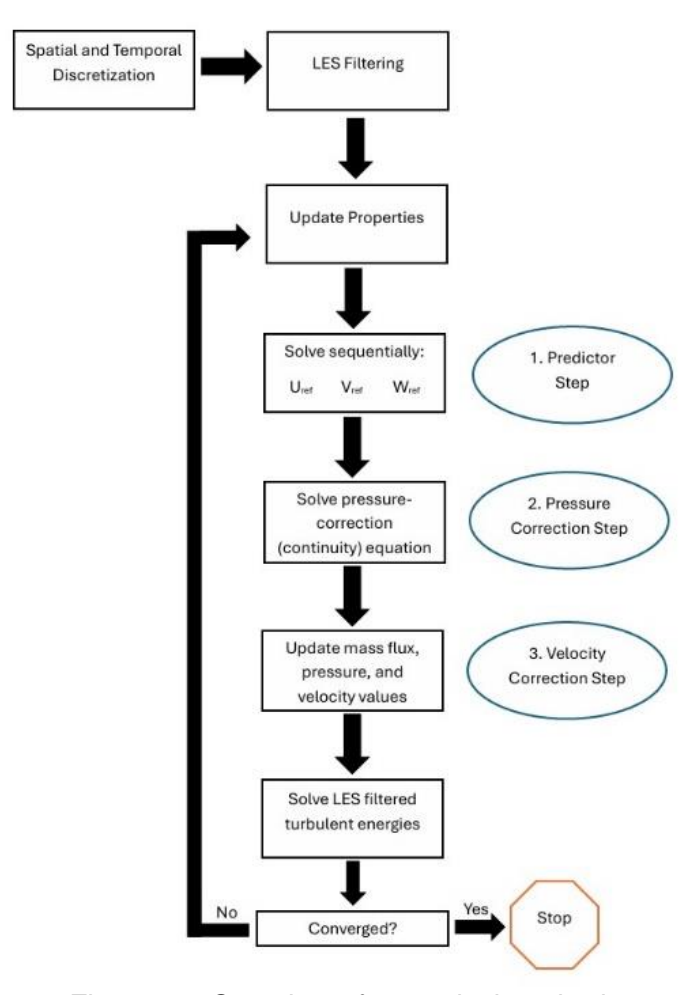


Figure 1 – Overview of numerical methods

2.3 Finite Element Analysis and System Coupling

The mechanical mesh of the parachute structure must be solved in addition to the fluid mesh. Force and displacement data values are exchanged between the fluid and mechanical solvers via system coupling. This represents the Fluid-Structure Interaction (FSI) of the parachute simulation since both Computational Fluid Dynamics (CFD) and Finite Element Analysis (FEA) are required to model the deforming fabric within the fluid flow with respect to time [12]. The mechanical mesh is spatially discretised to create an additional equation of motion, seen in Eq. (10).

$$[M]\{\ddot{x}(t)\} + [C]\{\dot{x}(t)\} + [K]\{x(t)\} = \{F^a(t)\}$$
(10)

Where M is the mass matrix, C is the damping matrix, K is the stiffness matrix, F^a is the applied load vector, and x is displacement followed by velocity and acceleration for its respective derivatives. This equation of motion is solved using a combination of the backward Euler, Eq. (11), and Newton-Raphson methods, Eq. (12):

$$\{\dot{u}_{n+1}\} = \frac{(\{u_{n+1}\} - \{u_n\})}{\Delta t} \tag{11}$$

$$[K_i^T]\{\Delta u_i\} = \{F^a\} - \{F_i^{nr}\}; \{u_{i+1}\} = \{u_i\} + \{\Delta u_i\}$$
(12)

where K_i^T is the Jacobian Matrix, and F_i^{n} is the internal force vector. These numerical methods work by first guessing an initial displacement value to calculate the Jacobian matrix and internal force vector. Then the change in the displacement vector is calculated and added to the original displacement amount for the next approximation. This process is repeated until the solution converges. The right-hand side of the Newton Raphson equation represents the residual. As this value approaches zero, the converged solution is computed. By sharing the converged values for both the fluid domain and parachute mesh, the interaction between the fluid and fabric is more easily calculated, thereby providing a more accurate representation of the fluid's effect on the unfurling parachute. This is achieved by matching the elements of the coupled fluid and structural meshes of the model with the Binary Space and Partitioning Algorithm [13], which recursively splits the source region into cells that contain source mesh locations, or "leaf cells". The algorithm continues until the maximum number of leaf cells is reached, at which point the target mesh locations are matched to each leaf cell to transfer data, displayed in Figure 2. The Profile-Preserving Mapping algorithm [13] uses shape functions to transfer intensive data such as displacement and temperature, while Conservative Mapping uses the "Intersect-Scatter-Gather" [13] method to transfer extensive data such as force, mass flow and heat rate. By utilizing these element matching methods, data from local source mesh elements can be summed when transitioning from the varying fluid and mechanical meshes.

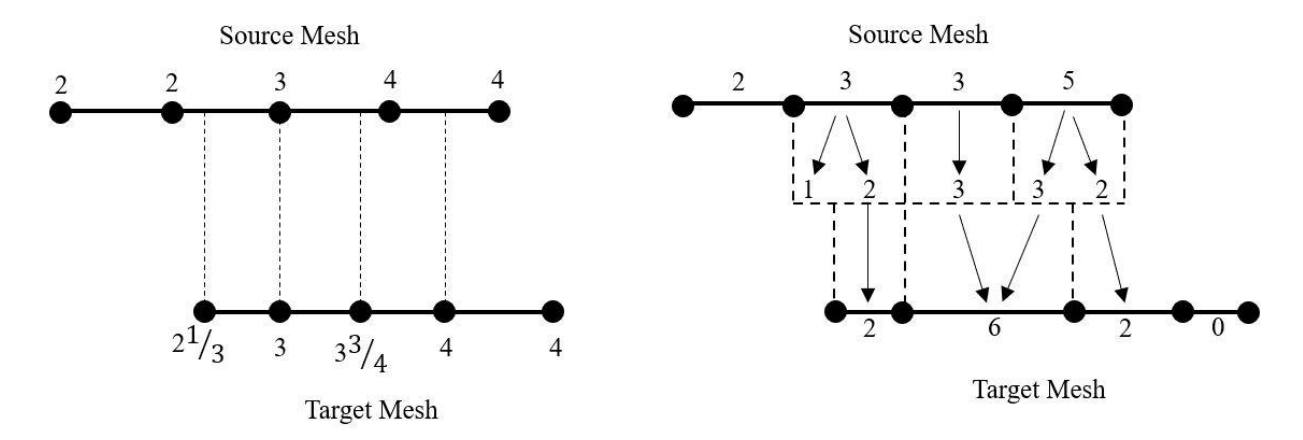


Figure 2 – Shape function (left) and conservative mapping (right)

2.4 Contact Algorithms

Since the fluid flow directly interacts with the deformable structure, contact numerical models are required. Contact is maintained when there exists no penetration/clipping between two bodies and momentum is conserved. The two main forms of contact algorithms are penalty-based and Lagrangian [14]. Penalty formulation utilises contact stiffness in the normal and tangential directions to resist the bodies from penetrating each other as if they were separated by a spring [15]. The stiffness is determined by the material properties of the structure and fluid. In the simulations, either Kevlar or mylar was used as the parachute material while air was always chosen as the working fluid. Not only do these materials accurately represent a parachute in a proper atmospheric environment, but the parameters are well-known to better model the contact stiffness. Lagrangian formulation on the other hand treats the contact of the materials as a constraint, thereby wholly preventing penetration [16]. When modelling an unfurling parachute with folds, wrinkles and overlapping fabric, penetration must be kept to a minimum to avoid fabric impingement. However, Lagrangian formulation is computationally expensive and can over-constrain the material to the point where it does not have the freedom to behave like a deformable fabric. Initial tests used just penalty-based constraints which produced failed results. As the swirling turbulent fluid forces open the slack parachute, the fabric begins to unfurl, but the penalty-based contact algorithm is unable to prevent the outer edges of the parachute canopy from folding in on the inner section of the canopy. Thus, the elements of the fabric pass through one another until the simulation ultimately fails.

To limit fabric penetration whilst reducing computational time, a hybridised Penalty-Lagrangian contact algorithm was used for the FSI simulation. By setting a hard cutoff for penetration slightly above the zero value at 0.1, the fabric impingement is reduced at only a moderate cost to computational time. Additionally, to reinforce the fabric and increase the contact stiffness, the parachute was modelled as a "sandwich-type structure" with two thin shell layers covering embedded cables that improved stiffness and the shape of the parachute. Verification of this contact algorithm is demonstrated in Figure 3 in a simple fabric sheet, metal rod drop test. In the drop test, a malleable sheet of Kevlar was suspended above an aluminium rod. The simulation was initialised, and gravitational forces were allowed to pull the fabric down above the fixed metal bar. With the updated hybridised contact algorithm model, the fabric elements were allowed to interact with the elements of the aluminium bar and with other elements of the fabric through folding. The fabric bends and conforms to the shape of the cylindrical bar through the penalty-based portion of the contact algorithm, without being allowed to pass through one another through the Lagrangian section of the hybridised model.

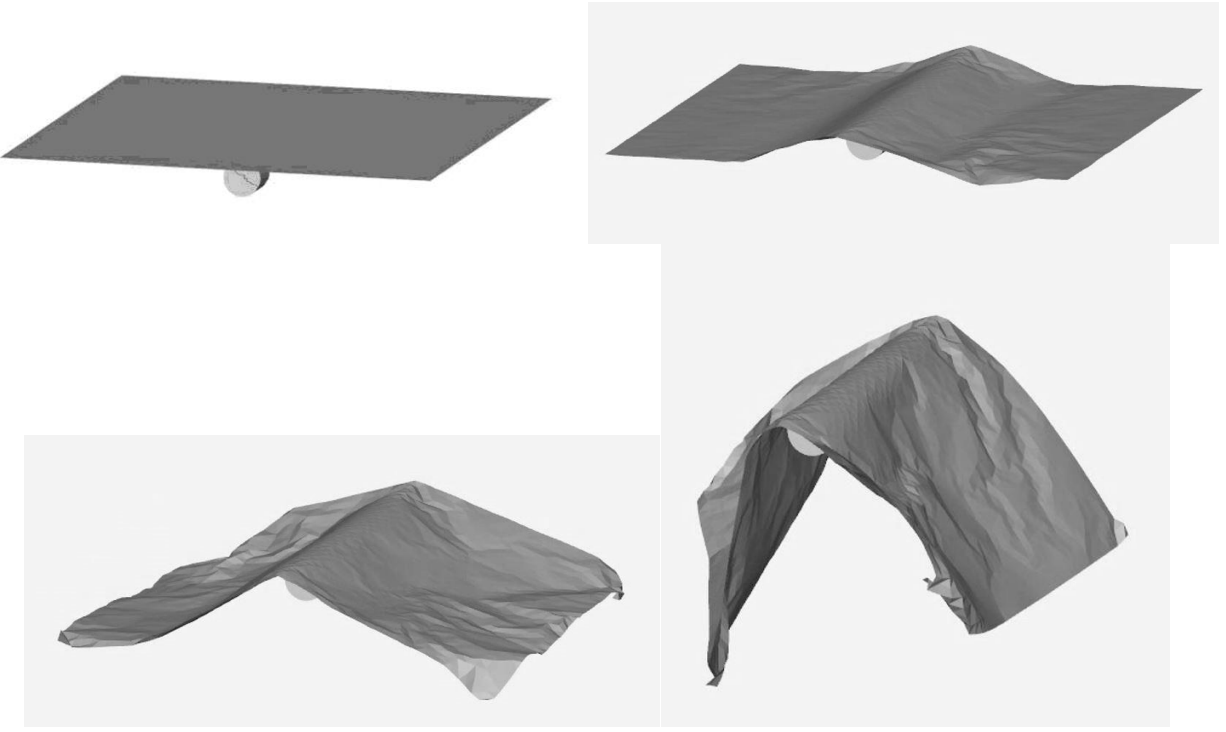


Figure 3 – Contact algorithm fabric test

2.5 Soft-body Cloth Modelling

The hybridised contact algorithm limits fabric impingement in the simulation, but further work is required to accurately simulate fabric deformation in a freestream. Because the model is allowed to deform, the relative distance between two points on the canopy is not fixed and changes with time. However, the overall shape of the parachute still needs to retain its basic form. Initially, to save on computational time, geometric-based techniques were attempted to simulate the parachute fabric. Utilising Weil's technique [17], the slack parachute was represented by a hanging cloth as a rigid grid with catenary curves between the hanging restraint points. This allows for straight diagonal lines on the 2D grid to be simplified by the catenary curves. The cloth shape is then further restrained with a relaxation algorithm that puts a limit on the distance points can travel within a certain amount of time [17]. These initial techniques are demonstrated in the early fabric and cable testing shown in Figure 4. A simple square of Kevlar is attached to a parachute cable along the diagonal line. The cable end is anchored to a fabric element while the cable itself is treated as a rigid spring capable of tension, but not compression. At 0 s, both the fabric and cable have incurred no deformation. However, after a tensile force is applied to the end of the cable, both the cable and fabric experience deformation at the 0.5 s mark.

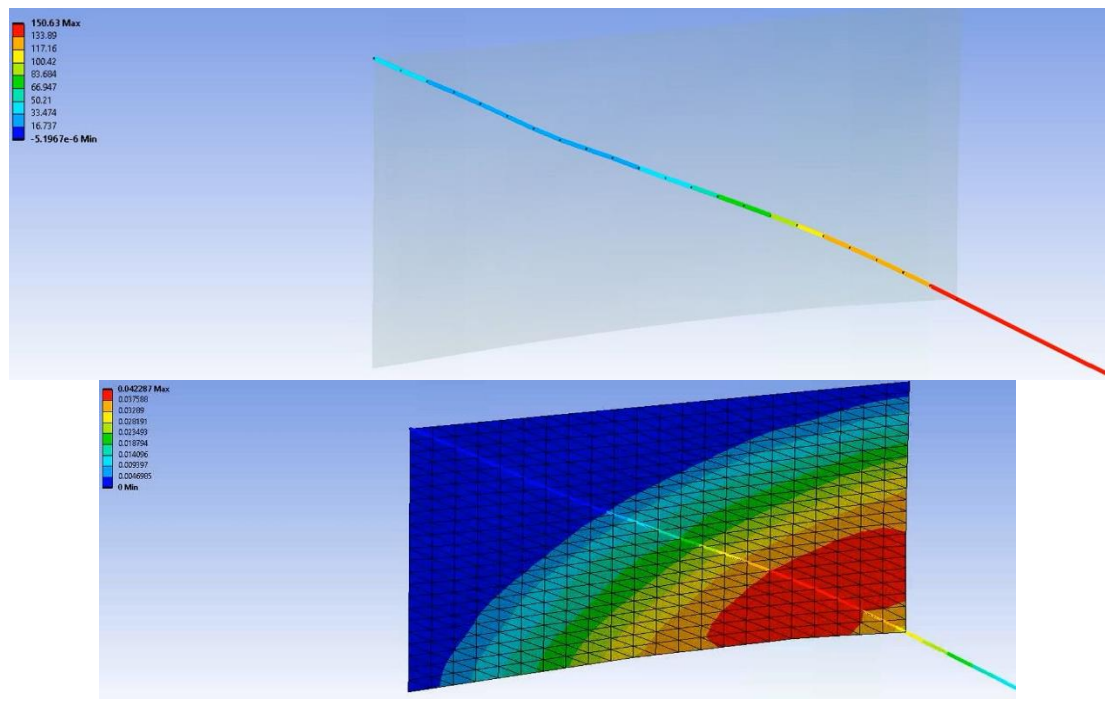


Figure 4 – Preliminary fabric stretch test

Weil's technique proved that deformable fabric and cables could be modelled in the commercial CFD software but that it was only robust enough to simulate simple soft body dynamics, as it is a vast oversimplification of the FSI physics involved in parachute inflation. A physical-based particle model is therefore required, where the cross-sectional fibers of the fabric are represented by the quadrilateral elements of the structural mesh. The total energy of the model is summarised in Eq. (13), where the gravitational energy is ignored in simulations representative of wind tunnel testing.

$$U_{total} = U_{repel} + U_{stretch} + U_{bend} + U_{trellis} + U_{gravity}$$
 (13)

Here, U_{repel} is the artificial energy of repulsion to keep a minimum distance between particles. $U_{stretch}$ is energy due to tensile strain. U_{bend} is energy caused by threads of the cloth bending out of the cloth plane. And $U_{trellis}$ represents energy due to shear strain. The total energies are solved for each element across a transient case and dictate the displacement of each structural element at each time step. The ability to accurately model deformable fabrics can then be further expanded upon by applying cloth modelling to a full-scale parachute inflation simulation.

2.6 Comparable Computational Methods

The Team for Advanced Modelling and Flow Simulation (T*AFSM) [18] utilised the Deforming-Spatial-Domain/Stabilized Space-Time (DSD/SST) model to study ring-sail parachutes. Their formulation improved parachute FSI whilst reducing computational time through the implementation of geometrical symmetry [19]. Additionally, T*AFSM performed studies on the lesser-known effects of drag produced by parachute cables. Their simulations proved that the inclusion of line drag created less than a 1% difference in total drag on the system when compared to simulations that ignored the cables [19]. This confirmation allowed for the line drag to be removed in this study since it was proven to have a negligible effect on the simulation.

The Farhat Research Group Laboratory also made advanced strides in using Finite Volume Method with Exact Two-phase Reimann (FIVER) solvers [20]. This method was used to model the Curiosity Rover parachute [21] and has been utilised to help with the permeable membrane study in this paper. Although specialised numerical solvers provided insight into parachute modelling, they can still only model stable descending parachutes after the inflation process has already occurred. During the literature review, the amount of documentation found on simulating fully packed to fully deployed parachutes was minimal. Therefore, the study focused on bridging the gap by first modelling a flat deflated parachute to a fully deployed state to contribute to the aerodynamic decelerator modelling area of research. Improving numerical modelling of the unfolding and inflation portions of the parachute deployment process is a worthwhile area of study. Although this section of the process is crucial to the functionality of the parachute, most data comes from costly experimental testing. By simulating the entire parachute inflation, the deployment process can be better studied to reduce the likelihood of failed parachute deployments that can cause the loss of supplies, vehicles, and human lives.

3. Methodology

Parachutes come in four basic shapes: cruciform, parafoil, annular and hemisphere. The two most common parachute types for decelerating payloads in the aerospace industry are annular and hemispherical. Therefore, these two designs were chosen to be simulated. Specifically, the hemispherical Air Force parachute from Technical Report 5867 [2], and the annular Mars Curiosity Rover parachute designs were chosen to model for validation based on the extensive experimental data available for each. In the absence of specific dimensions, it was estimated that the Air Force parachute was a 10% extended skirt hemispherical parachute with a surface area of $A_S = 10.32 \text{ m}^2$, a radius of r = 1.1 m, and a line length of l = 2.17 m. The parachute cables were modelled as onedimensional springs that experience tensile forces, but not compression. The parachute fabric was meshed utilising shell elements, with embedded reinforcement cables sandwiched between two thin membranes of thickness t = 1.02e-5 m. The parachute material was chosen to be MIL Type III [22] due to its well-known parameters and wide use within the field. The annular Curiosity parachute was modelled similarly to the Air Force parachute, but with a radius of r = 8.0 m, line length of l = 16 m, and a parachute ribbon with a disk gap band of 0.4 m. A refined fluid mesh was created near both parachutes using a 2.54 m diameter sphere and a 5.08 m long cylinder downwind of the parachute. The fluid domain, parachute geometry and boundary meshes are visualised in Figure 5 for the Air force parachute. The element size for the mechanical mesh was kept equivalent to the fluid mesh size, except for the mesh boundaries near the parachute walls. To ensure grid independence, a mesh refinement study was conducted for ten iterations to ensure convergence, as displayed in Figure 6. The final element count used achieved less than 0.5% error where it was determined that a mesh element size of 2.3 cm for the Air Force parachute, and 1.25 cm for the Curiosity parachute converged to a stable total drag.

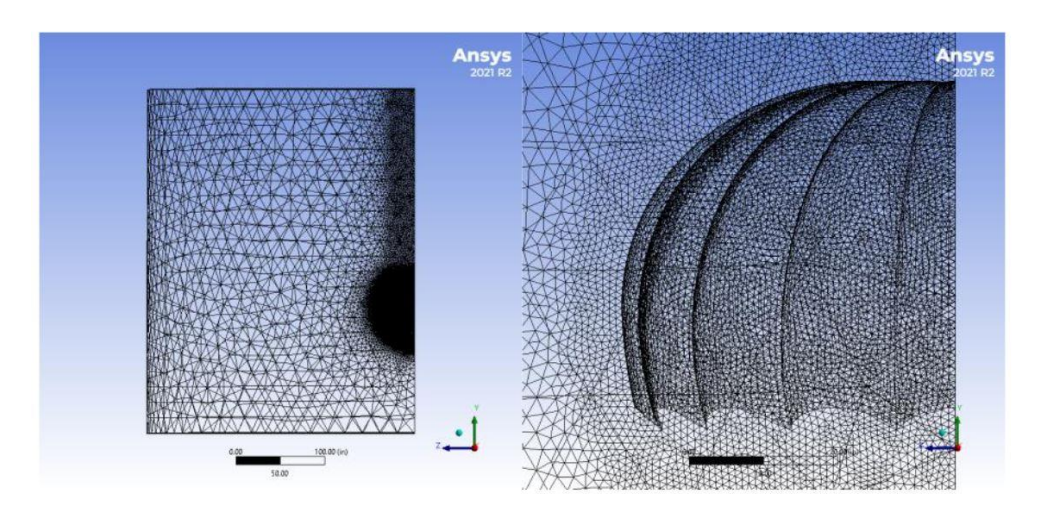


Figure 5 – Air force parachute control volume

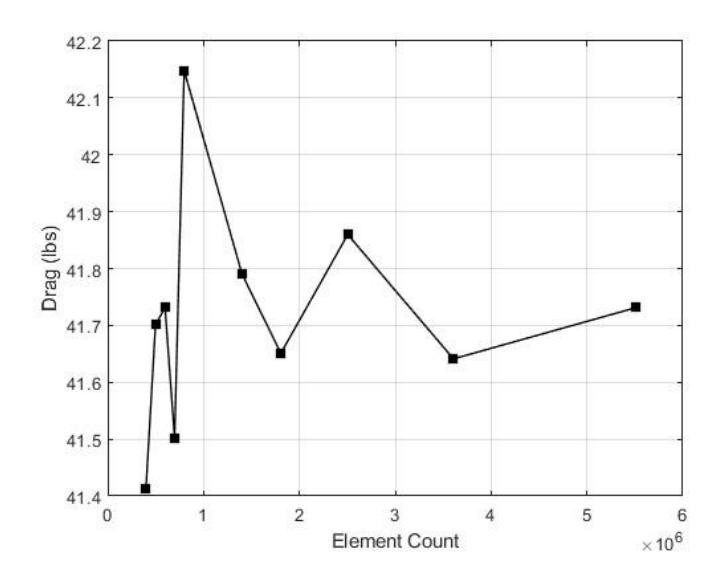


Figure 6 – Air force parachute mesh refinement study

Following the creation of the parachute geometry and meshing, the fluid field underwent 1 s of initialisation where the parachute was held stationary to create initial conditions for the simulation. The PISO and LES numerical methods were used with a time step size of 0.0001 s, 6 maximum iterations per time step, and a total simulation time of 4 s. At each time step, the flow solver calculated the velocity for each fluid element, with the solid solver then determining the stress on each structural element. From this, the parachute position, drag coefficient and total drag were recorded for multiple cases of fluid velocity and fabric permeability. Finally, the overall inflation was measured through the visualisation of the simulation results and compared for accuracy against the experimental inflation values.

4. Results

The porous jump condition was used to model thin permeable membranes. The parachute fabric is not a solid wall and has a certain porosity that allows for the fluid flow to partially pass through it. The value used was verified against experimental numbers for the Air Force parachute at four different entry velocities, tabulated in Table 1 and plotted in Figure 7. Additionally, the total drag force with respect to time on the parachute canopy was measured for the duration of the parachute inflation process.

Velocity (m/s)	Wall Boundary	Porous-Jump Condition	Exper. PJC Value
3.63	0.7271	N/A	0.845
5.39	0.7089	0.6802	0.766
8.90	0.7124	0.6668	0.686
13.78	0.7027	0.6489	0.7

Table 1 – Air force parachute drag coefficient table

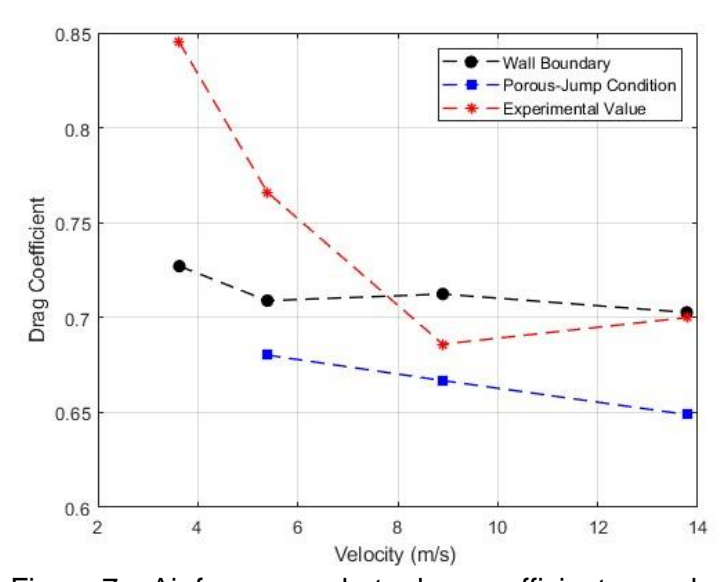


Figure 7 – Air force parachute drag coefficient vs. velocity

Compared to the experimental drag coefficients, the simulation of the Air Force parachute showed a maximum error of 10% for the lower deployment velocity, and a minimum error of 2.7% for the higher deployment velocity of 8.90 m/s. The difference could be explained by the lack of full inflation and fabric impingement that occurs at a lower deployment velocity. The simulated drag force was within the range of the experimental values, and likewise displayed periodic oscillations that corresponded to the parachute swaying and then tapering off as the parachute regained stability. This is seen in Figure 8, where an element's location (yaw angle) near the top vent hole of the Air Force parachute is tracked with respect to time over the course of the simulation.

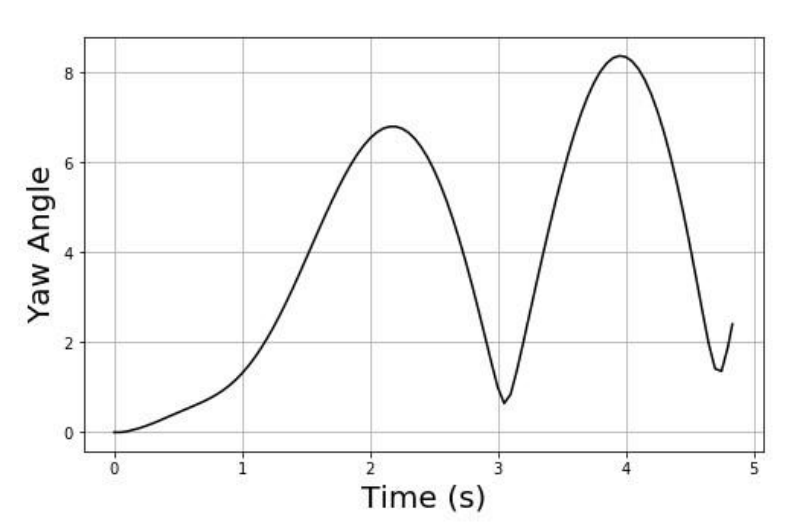


Figure 8 – Air force parachute element location sway

The Curiosity parachute inflation was also simulated in a fluid environment but was allowed to inflate over the time period that was documented in its Mars entry log. Before testing the inflation of the fabric, a stationary Curiosity parachute model was initialised in a fluid domain representative of entry into the Martian atmosphere. As evident in Figure 9, the velocity of the flow is greatest in magnitude in the area surrounding the parachute canopy. This is because the flow does not get blocked by the incident fabric of the parachute. The next highest velocity areas are the "internal area" of the canopy and the area immediately downstream of the vent hole. This proves that the model is correctly simulating the entry environment and will produce accurate boundary conditions. Additionally, the initialisation also proves that the porosity of the parachute membrane is properly calibrated.

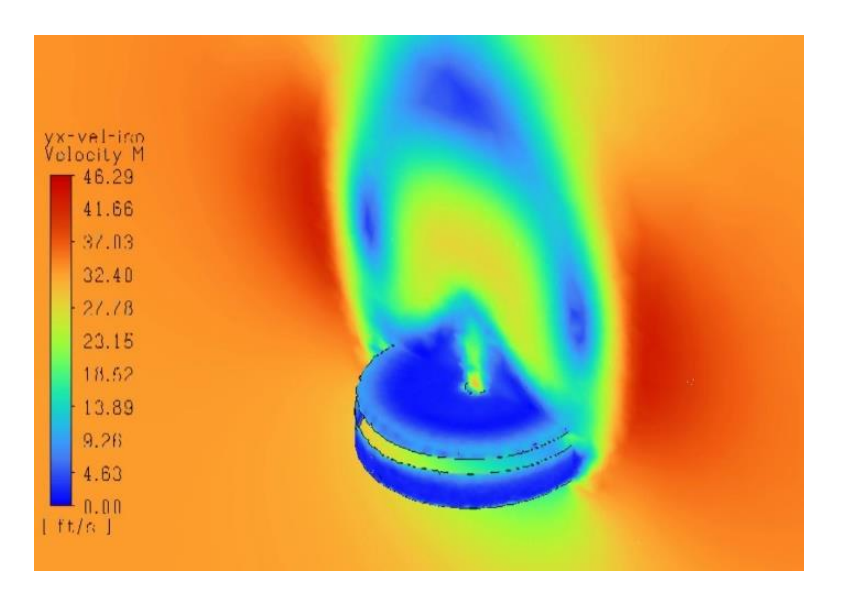


Figure 9 – Curiosity parachute surrounding flow

After initialisation, the inflation process is carried out in the commercial CFD software for a 1 s timeframe. At the start of the simulation the deflated parachute geometry is deformed by the subsonic air stream. This causes the fabric to deform in the turbulent flow wake. When a critical mass of air enters the internal parachute geometry, it begins to push outward on the fabric, causing it to inflate around the 0.2 s mark. The first figure (top left) in Figure 10 is the slack parachute at the start of the simulation when the fluid flow is initialised. At this point in time, the fluid flow has not exerted any substantial force on the fabric and although stresses have already begun to form, the shape of the parachute is yet to undergo any major deformation. A flat deflated parachute is used in the interim while further progress is being made on modelling a fully folded parachute. The flat form provides an accurate starting point before the fabric is deformed by the fluid. One method of improving parachute folding to limit fabric impingement is to utilise Коряпин – Митюрьев (Korjapin – Mitiuriev) folding methods, to reduce the amount of fabric overlap during the packing stage.

When the fluid flow is first introduced to the parachute membrane, the canopy, pushed by the air, starts to form a more concave shape. However, the *Re* of the initial flow increases and becomes more turbulent as it interacts with the structure of the parachute. As shown in the top right and bottom left figures of Figure 10, the more turbulent air trapped in the parachute canopy begins to affect the fabric. As the flow stabilises, the parachute reaches its final inflated shape in the bottom right figure of Figure 10. Figure 10 displays the inflation process as captured by the CFD post-processor with stress contouring. Figure 11 on the other hand, is created by importing the Air force parachute canopy and cable position data into a separate graphical software. This allows for the parachute inflation process to be seen at a higher quality, but with the same data calculated utilising the applied turbulence models.

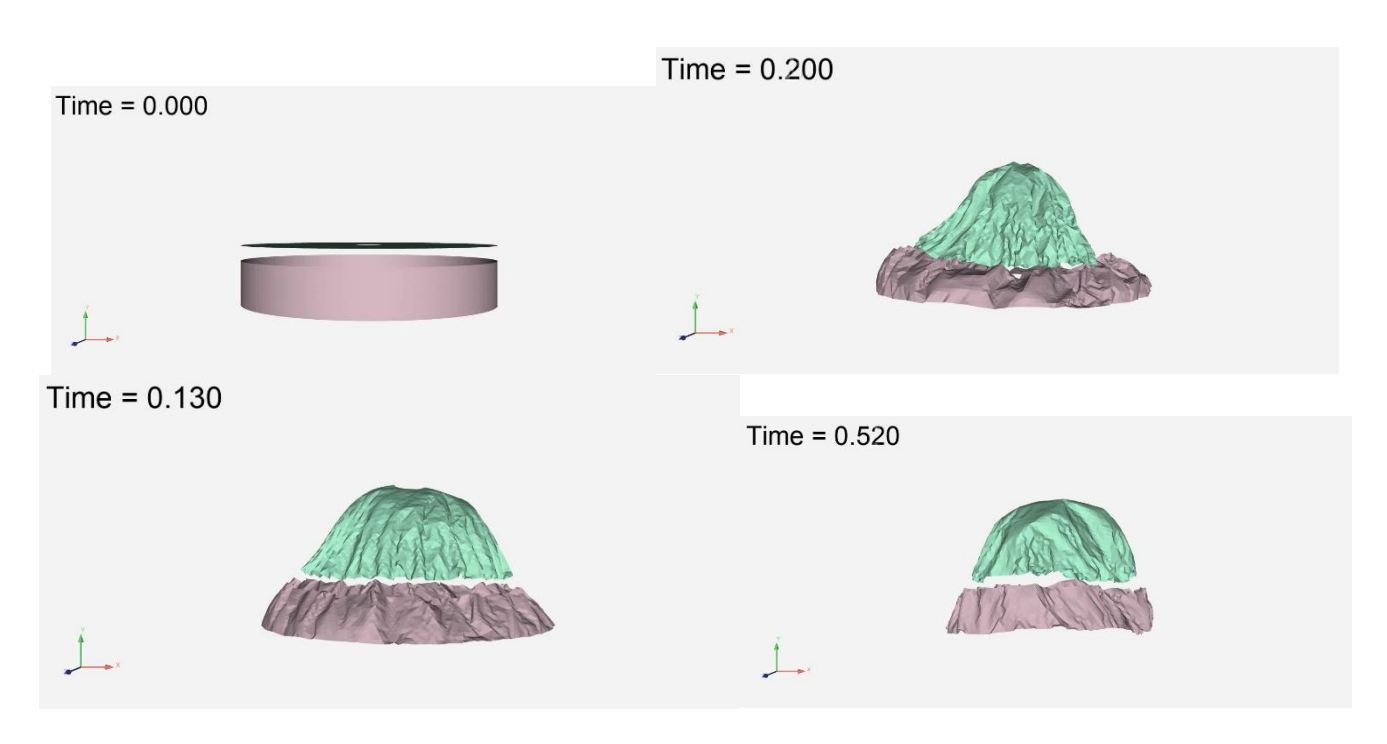


Figure 10 – Curiosity parachute inflation side view

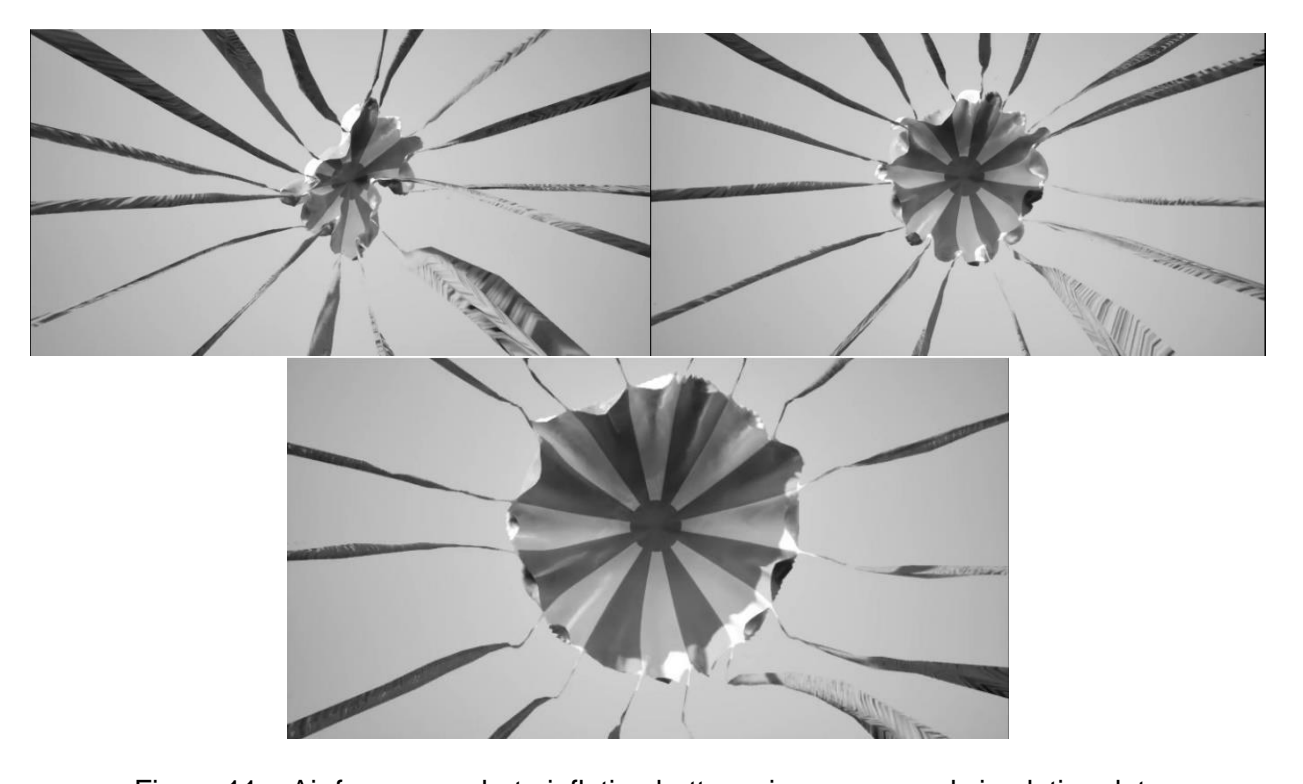


Figure 11 – Air force parachute inflation bottom view processed simulation data

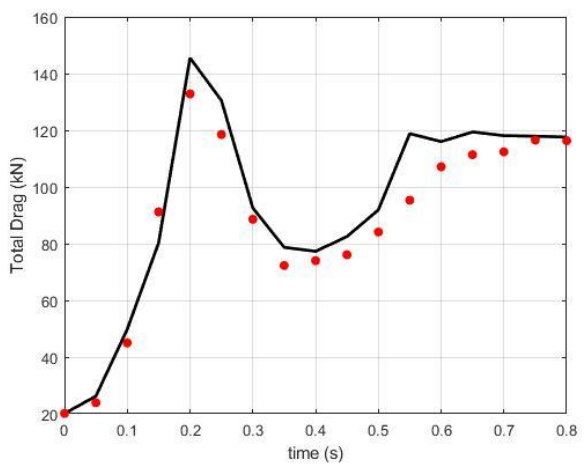


Figure 12 – Curiosity parachute inflation vs. experimental curiosity inflation data

The experimental data from the Mars Curiosity parachute deployment was then compared to the total drag calculated on the simulation parachute canopy, plotted in Figure 12. Compared to the tests, the simulation displayed a similar drag trend with an average error of 8.3%. Additionally, both the simulation and physical parachutes experienced total stable inflation at the same 0.8 s mark, when total drag stabilised. Although most previously documented parachute simulations model the stable descent stage of the parachute, this simulation gives accurate inflation data across a valid timeframe, from a flat-slack initial stage to the beginning of stable descent after the inflation process.

5. Conclusion

User defined FSI algorithms within commercial software with appropriate turbulence models, were developed and utilised with the aim to achieve an accurate representation of parachute inflation from flat to fully inflated. Drag force and inflation time values were comparable to the experimental data from two different landmark parachute trials. Additional work was devoted to the implementation of a hybridised contact algorithm to limit fabric impingement, and a soft body dynamic model to improve fabric deformation. Additionally, the visual models of the inflation process were very similar to real-time parachute inflation images. By improving parachute inflation techniques, the accuracy of parachute deployment simulations is further enhanced to reduce the need for costly parachute experiments. Future work will focus on incorporating additional algorithms with the aim of reducing fabric impingement and simulating inflation from a fully packed state.

6. Acknowledgements

The completion of this study would not have been possible without the expertise of the team within the *CRASH* Lab, including Cameron Grace, Louis Rizzo, and Steven Herrera.

7. Contact Author Email Address

Mail to: bayandor@buffalo.edu

8. Copyright Statement

The authors confirm that they, and/or their company or organization, hold copyright on all the original material included in this paper. The authors also confirm that they have obtained permission from the copyright holder of any third-party material included in this paper, to publish it as part of their paper. The authors confirm that they give permission or have obtained permission from the copyright holder of this paper, for the publication and distribution of this paper as part of the ICAS proceedings or as individual off-prints from the proceedings.

References

- [1] Lenormand L. S and Maigne W. Les Arts de L'assembleur du Satineur, du Brocheur, du Rogneur. Encyclopedie Roret, Paris, France, 1932.
- [2] Stimler F. J and Ross R. S. Drop Tests of 16,000-Square-Inch Model Parachutes. Vol. 1, 1960.
- [3] Gambele J. D. A Mathematical Model for Calculating the Flight Dynamics of a General Parachute-payload System. Legacy CDMS, 1968.
- [4] Dawoodian M, Dadvand A and Hassanzadeh A. A Numerical and Experimental Study of the Aerodynamics and Stability of a Horizontal Parachute. *ISRN Aerospace Engineering*, Vol. 2013, pp 1-8, 2013.
- [5] Knacke T. W. *Parachute Recovery Systems Design Manual*. Para Publishing, Santa Barbara, CA, 1991.
- [6] Zumwalt C. H, Cruz J. R, Keller D. F and O'Farrell C. *Wind Tunnel Test of Subscale Ringsail and Disk-Gap-Band Parachutes*. Langley Research Center, Hampton, VA, 2016.
- [7] Maydew R. C and Peterson C. W. Design and Testing of High-Performance Parachutes (Advisory Group for Aerospace Research and Development). Specialised Printing Services Limited, 1991.
- [8] Poinsot T and Veynante D. *Theoretical and Numerical Combustion*. 2nd edition, Philadelphia: Edwards, 2005.
- [9] Smagorinsky J. General Circulation Experiments with the Primative Equations: I. The Basic Experiment. *Monthly Weather Review*, Vol. 91, No. 3, pp 99-164, 1963.
- [10] Xiao F. Unified Formulation for Compressible and Incompressible Flows by Using Multi-integrated Moments I: One-dimensional Inviscid Compressible Flow. *Journal of Computational Physics*, Vol. 195, No. 2, pp 629-654, 2004.
- [11] Ansys Academic Research Mechanical, Release 18.1, Help System, Pressure-Velocity Coupling Method. ANSYS, Inc, 2024.
- [12] Horton B, Song Y, Feaster J and Bayandor J. Benchmarking of Computational Fluid Methodologies in Resolving Shear-Driven Flow Fields. *Journal of Fluids Engineering*, Vol. 139, No. 11, 2017.
- [13] Karlsson R, and Lingas A. SWAT 88. 1st Scandinavian Workshop on Algorithm Theory, Halmstad, Sweden, 318, 1988.
- [14] Ager C, Seitz A and Wall W. A. A Consistent and Versatile Computational Approach for General Fluid-structure-contact Interaction Problems. *International Journal for Numerical Methods in Engineering,* Vol. 122, No. 19, pp 5279-5312, 2021.
- [15] Xiao Y and Liu K. 3D Surface-to-Surface Contact Algorithm for SPH Method and Its Application to Simulation of Impact Failure of Ceramic Plate. *Applied Sciences*, Vol. 13, No. 6, pp 3790, 2023.
- [16] Bai X, Sun J and Zheng X. An Augmented Lagrangian Decomposition Method for Chance-Constrained Optimization Problems. *INFORMS Journal on Computing*, Vol. 33, No. 3, pp 1056-1069, 2021.
- [17] Babic K. Cloth Modeling. Indian Institute of Technology, Bombay, India, 1999.
- [18] Tezduyar T. E, Sathe S, Schwaab M, Pausewang J, Christopher J and Crabtree J. Fluid-structure Interaction Modeling of Ringsail Parachutes. *Computational Mechanics*, Vol. 43, No. 1, pp 133-142, 2008.
- [19] Bazilevs Y, Takizawa K and Tezduyar T. E. *Computational Fluid-Structure Interaction: Methods and Applications*. 1st edition, Hoboken: Wiley (Wiley series in computational mechanics), 2012.
- [20] Farhat C, Gerbeau J. F and Rallu A. FIVER: A Finite Volume Method Based on Exact Two-phase Riemann Problems and Sparse Grids for Multi-material Flows with Large Density Jumps. *Journal of Computational Physics*, Vol. 231, No. 19, pp 6360-6379, 2012.

FSI MODELLING OF AERODYNAMIC DECELARATORS

- [21] Huang D. Z, Avery P, Farhat C, Rabinovitch J, Derkevorkian A and Peterson L. D. Modeling, Simulation and Validation of Supersonic Parachute Inflation Dynamics During Mars Landing. *AIAA Scitech Forum*, Vol. 1, 2020.
- [22] Cruz J. R, Mineck R. E, Keller D. F, and Bobskill M. V. *Wind Tunnel Testing of Various Disk-Gap-Band Parachutes*. Langley Research Center, 2003.